International Journal of Bifurcation and Chaos, Vol. 36, No. 7 (2026) 2650087 (15 pages)

DOI: 10.1142/S0218127426500872

A Novel Circulant System with Six Coexisting Symmetric Conservative Chaotic Seas

Karthikeyan Rajagopal
Center for Research, Easwari Engineering College, Chennai, India
Center for Cognitive Science, Trichy SRM Medical College Hospital and Research Center, Trichy, India
Center for Research, SRM TRP Engineering College, Trichy, India
rkarthiekeyan@gmail.com

Fahimeh Nazarimehr*
Department of Biomedical Engineering, Amirkabir University of Technology (Tehran Polytechnic), Tehran, Iran
f_nazarimehr@aut.ac.ir

Sajad Jafari
Department of Biomedical Engineering, Amirkabir University of Technology (Tehran Polytechnic), Tehran, Iran
Health Technology Research Institute, Amirkabir University of Technology (Tehran Polytechnic), Tehran, Iran
sajadjafari@aut.ac.ir

Julien C. Sprott
Department of Physics, University of Wisconsin–Madison, Madison, WI 53706, USA
csprott@wisc.edu

Received September 29, 2025; Accepted January 5, 2026; Published February 9, 2026

This study presents a new three-dimensional circulant chaotic system with both conservative and dissipative dynamics. It is characterized by six coexisting symmetric seas. The system's governing equations exhibit circulant symmetry, ensuring invariance under cyclic permutations of variables, and incorporate cubic nonlinearities that give rise to complex dynamics. Through a detailed analysis, we demonstrate the system's rich behavior, including equilibrium points, bifurcations, Lyapunov exponent spectra, and the region occupied by the chaotic sea structures. The dynamics are distinct in their regions of initial conditions, highlighting the multistability. Bifurcation analysis reveals transitions between chaotic, periodic, dissipative, and conservative regimes, while Lyapunov exponents confirm the existence of conservative and dissipative dynamics. The extent of the chaotic seas exhibits sharp boundaries of chaotic dynamics which

*Author for correspondence

are discussed mathematically. Also, it shows embedded quasi-periodic invariant tori, further enriching the system's complexity. This work advances the understanding of symmetric chaotic systems.

Keywords: Circulant symmetry; chaotic flow; multistability; conservative dynamics.

1. Introduction

Chaotic systems have long captivated researchers due to their rich dynamical behavior and wide-ranging applications, including secure communication [Li *et al.*, 2020a; Obaid *et al.*, 2025; Xu *et al.*, 2023a], random number generation [Kopparthi *et al.*, 2022; Tamba *et al.*, 2025], and neural modeling [Chen *et al.*, 2025; Bao *et al.*, 2025; Vignesh *et al.*, 2025]. Neural circuits have attracted significant attention in this context [Xu *et al.*, 2023b; Xu *et al.*, 2023c; Xu *et al.*, 2020]. One of the defining features of chaos is its sensitivity to initial conditions, which gives rise to complex, unpredictable trajectories that are deterministic in nature [Sprott, 2010]. Over the years, various classes of chaotic systems have been explored [Barathi *et al.*, 2025; Wang *et al.*, 2024], including those with no equilibrium points [Yang *et al.*, 2021] and multiple coexisting attractors [Vaidyanathan *et al.*, 2021]. Among these, symmetric systems offer unique insights into the interplay between structure and dynamics [Wang *et al.*, 2022].

The topology of attractors in chaotic flows is significantly influenced by symmetry. In particular, rotational or permutation symmetry can lead to the emergence of attractors that are related through symmetry transformations [Xu *et al.*, 2023b]. These attractors often exhibit elegant spatial arrangements, making them of interest from both theoretical and practical perspectives [Li *et al.*, 2020b]. Circulant systems, characterized by equations that remain invariant under cyclic permutations of the state variables, are recognized as an important subclass of symmetric chaotic systems [Sprott, 2010]. The structured dynamics of such systems render them particularly suitable for analytical studies and real-world implementations [Yousfi *et al.*, 2024]. Recent studies have reported chaotic systems with multiple coexisting attractors arranged under various types of symmetry [Azam *et al.*, 2022].

To the best of our knowledge, the system presented in this paper is the first Three-Dimensional (3D) autonomous chaotic flow with circulant symmetry to exhibit six coexisting conservative chaotic seas, organized into two symmetry-related groups. Each sea originates from a distinct basin of attraction, yet all maintain topological equivalence under cyclic permutations of the state variables — a direct consequence of the system's underlying symmetry. Remarkably, the boundaries separating these seas are sharp and mathematically well defined, in stark contrast to the typically fractal or riddled boundaries observed in multistable chaotic systems. We provide a rigorous geometric explanation for these boundaries by analyzing the unstable manifolds of saddle equilibrium points, establishing a direct link between local linearized dynamics and global phase-space organization — an approach not previously reported in the study of symmetric or circulant chaotic systems. Furthermore, the system displays a rich interplay between conservative and dissipative dynamics under parameter variation, hosting embedded quasi-periodic invariant tori alongside chaotic seas. These features collectively satisfy Sprott's second criterion for novelty [Sprott, 2011] — the exhibition of previously unobserved dynamical behavior — and underscore the system's significance as a new paradigm in the study of structured chaos.

This work is organized as follows: Sec. 2 presents the mathematical formulation of the system. Section 3 analyzes its dynamical behavior, including equilibria, phase portraits, bifurcations, and Lyapunov spectra. Section 4 investigates the regions occupied by the chaotic seas, and their boundaries are analyzed mathematically. Section 5 discusses the implications and possible applications of the observed dynamics.

2. Mathematical Model

This work describes a distinctive 3D-chaotic system defined by circulant symmetry, which accommodates six coexisting chaotic seas. The system incorporates cubic and quadratic nonlinearities. The combination of these two types of polynomial nonlinearities is deliberately chosen to balance structural simplicity with the capacity to produce rich, organized chaos. Through extensive numerical

exploration, we find that this specific blend enables the emergence of six coexisting conservative chaotic seas with sharp basin boundaries, a phenomenon that appears highly sensitive to the form and balance of nonlinear terms. The following are the system's governing equations:

$$\begin{aligned}\dot{x} &= a(y+z) + b(y^3+z^3) + c(y+z)x^2,\\ \dot{y} &= a(z+x) + b(z^3+x^3) + c(z+x)y^2,\\ \dot{z} &= a(x+y) + b(x^3+y^3) + c(x+y)z^2.\end{aligned} \tag{1}$$

The parameters are $a = 5$, $b = -1$, and $c = 1$. Since this system maintains circulant symmetry, every equation may be derived from the others by cyclically permuting the variables $x \to y \to z \to x$. Furthermore, the system exhibits symmetry about the origin, which means the equations have inversion symmetry $(x, y, z) \mapsto (-x, -y, -z)$. Such symmetries play a crucial role in the emergence of multiple symmetric dynamics. The nonlinear terms include cross-couplings, which contribute to complex stretching and folding mechanisms essential for generating chaotic behavior. Specifically, the terms $b(y^3 + z^3)$, $b(z^3 + x^3)$, and $b(x^3 + y^3)$ introduce strong nonlinearity, while the terms $c(y + z)x^2$, $c(z+x)y^2$, and $c(x+y)z^2$ modulate the interaction strength depending on the state of the system.

3. Dynamical Behavior and Analysis

The system's dynamical characteristics, encompassing equilibrium points, Lyapunov Exponents (LEs), and bifurcations, can be further examined using the formulation of the previous section, which serves as the basis for the discussion in the following.

3.1. *Equilibrium points and stability*

We start by examining the equilibria of the suggested model in order to comprehend its basic dynamical behavior. The temporal derivatives $\dot{x}$, $\dot{y}$, and $\dot{z}$ are set to zero to obtain these points:

$$\begin{aligned}a(y+z) + b(y^3+z^3) + c(y+z)x^2 &= 0,\\ a(z+x) + b(z^3+x^3) + c(z+x)y^2 &= 0,\\ a(x+y) + b(x^3+y^3) + c(x+y)z^2 &= 0.\end{aligned} \tag{2}$$

The parameters are $a = 5$, $b = -1$, and $c = 1$. Each equation is a cyclic permutation of the others because of the system's circulant symmetry. Accordingly, any solution (x_e, y_e, z_e) will have two additional solutions produced by cyclic permutations of its constituent parts. Also, for each equilibrium except $(0, 0, 0)$ (which is symmetric itself), each equilibrium has a dual with symmetry around the origin. By solving Eq. (2), 13 equilibria are shown in Table 1.

Table 1. Equilibrium points and their corresponding eigenvalues for the proposed system with parameters $a = 5$, $b = -1$, and $c = 1$.

Equilibrium	Coordinates (x, y, z)	Eigenvalues
Eq_1	(0, 0, 0)	-5, -5, 10
Eq_2	(-1.291, 2.582, 2.582)	15, $-7.5 \pm 11.99i$
Eq_3	(2.582, 2.582, -1.291)	15, $-7.5 \pm 11.99i$
Eq_4	(2.582, -1.291, 2.582)	15, $-7.5 \pm 11.99i$
Eq_5	(1.291, -2.582, -2.582)	15, $-7.5 \pm 11.99i$
Eq_6	(-2.582, -2.582, 1.291)	15, $-7.5 \pm 11.99i$
Eq_7	(-2.582, 1.291, -2.582)	15, $-7.5 \pm 11.99i$
Eq_8	(0, 0, 2.2361)	-5, $2.5 \pm 13.9194i$
Eq_9	(0, 2.2361, 0)	-5, $2.5 \pm 13.9194i$
Eq_{10}	(2.2361, 0, 0)	-5, $2.5 \pm 13.9194i$
Eq_{11}	(0, 0, -2.2361)	-5, $2.5 \pm 13.9194i$
Eq_{12}	(0, -2.2361, 0)	-5, $2.5 \pm 13.9194i$
Eq_{13}	(-2.2361, 0, 0)	-5, $2.5 \pm 13.9194i$

The Jacobian matrix is assessed at each equilibrium to determine its local stability. The following is the Jacobian matrix:

$$J = \begin{pmatrix} 2cx(y+z) & a+3by^2+cx^2 & a+3bz^2+cx^2 \\ a+3bx^2+cy^2 & 2cy(z+x) & a+3bz^2+cy^2 \\ a+3bx^2+cz^2 & a+3by^2+cz^2 & 2cz(x+y) \end{pmatrix}. \tag{3}$$

The Jacobian matrix is assessed at each fixed point, and the characteristic equation is then created by solving $\det(\lambda I - \mathrm{Jac}) = 0$. Each equilibrium's stability type is ascertained using the eigenvalues. The eigenvalues corresponding to each equilibrium point are presented in Table 1.

The eigenvalues show that there are both real and complex eigenvalues throughout the equilibria, suggesting a combination of spiral and nodal dynamics. All of the equilibrium points are saddle, having both negative and positive real parts in their eigenvalues. These unstable equilibria may serve as repellers, guiding trajectories into chaotic regions. The interplay between the equilibria is believed to contribute to the formation of the six coexisting seas discussed in subsequent sections.

3.2. *Phase portraits and the seas visualization*

Under the chosen parameter set $a = 5$, $b = -1$, and $c = 1$, the suggested system displays six different

Table 2. Initial conditions used to reveal the six coexisting chaotic seas and their corresponding color coding in phase portraits.

Label	Initial Condition (x_0, y_0, z_0)	Color
IC_1	(−4, 5.5, 2.4)	Azure
IC_2	(5.5, 2.4, −4)	Green
IC_3	(2.4, −4, 5.5)	Purple
IC_4	(0.54, 1.83, −2.26)	Blue
IC_5	(−2.26, 0.54, 1.83)	Black
IC_6	(1.83, −2.26, 0.54)	Red

chaotic seas that coexist in phase space, each associated with a specific set of initial conditions. The dynamics exhibit a symmetric configuration centered around the origin. The six selected initial conditions are as shown in Table 2.

Due to the circulant structure of the governing equations, all dynamics preserve the system's overall symmetry. This system exhibits a complex geometric structure of the dynamics, as illustrated in Fig. 1. The LEs of the chaotic dynamics are $(0.964, 0, -0.964)$. The sum of the LEs equals zero, so the dynamics are conservative, and they are called the chaotic seas.

The system exhibits two distinct groups of chaotic seas, each characterized by circulant symmetry, wherein the dynamics of one sea in a group can be derived from another through cyclic permutation of the variables. Also, the seas of the two groups are symmetric around the origin. These seas are illustrated in Fig. 2, where each group is separately visualized: the first column presents projections of the trajectories of each group onto the x–y plane, highlighting their symmetric spatial distribution in each group, while the second column displays their 3D structure. This dual representation emphasizes the complex orbital behavior of the

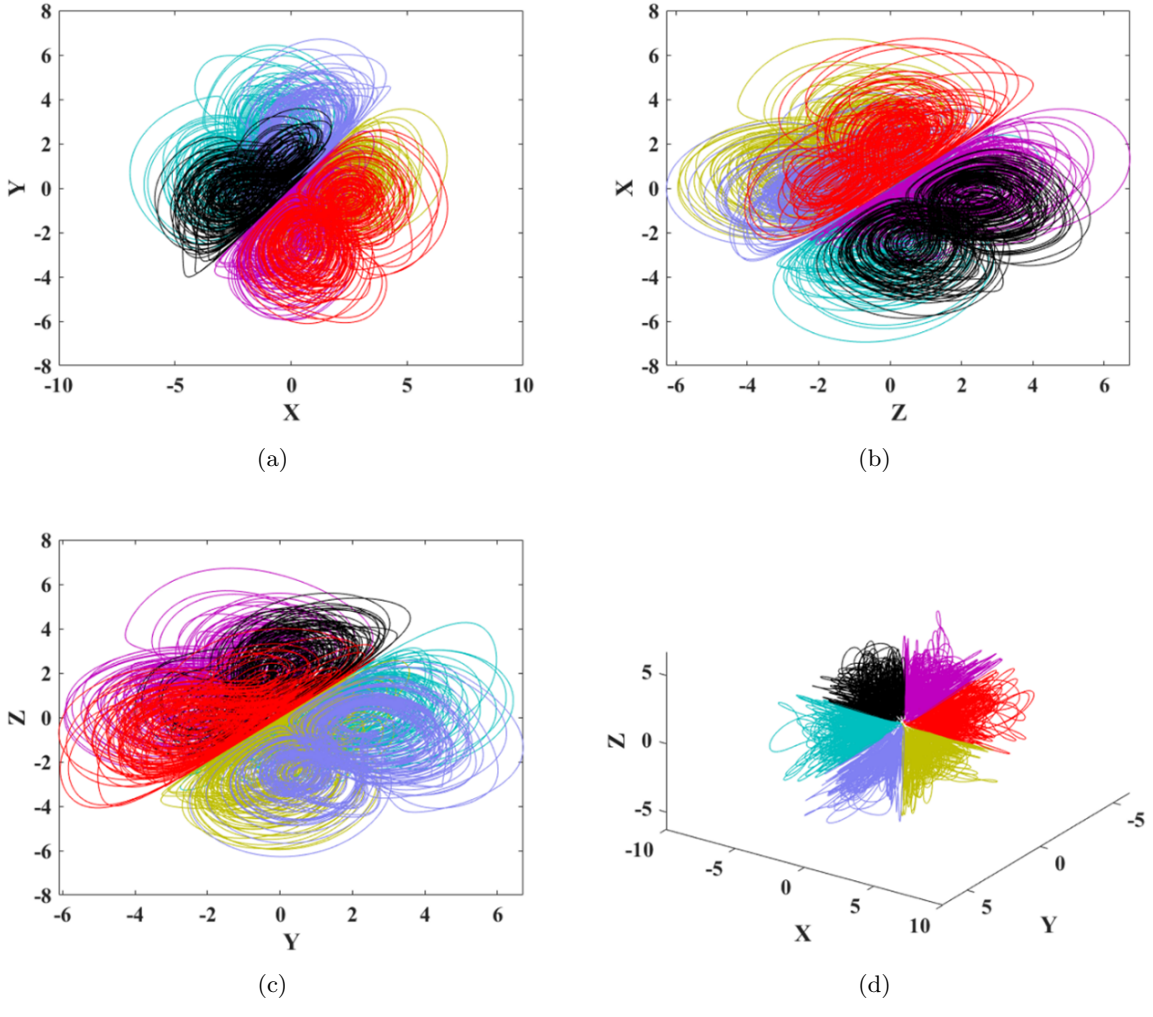

Fig. 1. Chaotic dynamics of Eq. (1) correspond to the initial conditions IC_1, IC_2, IC_3, IC_4, IC_5, and IC_6, colored by azure, green, purple, blue, black, and red, respectively, in (a) x–y plane; (b) z–x plane; (c) y–z plane and (d) x–y–z space.

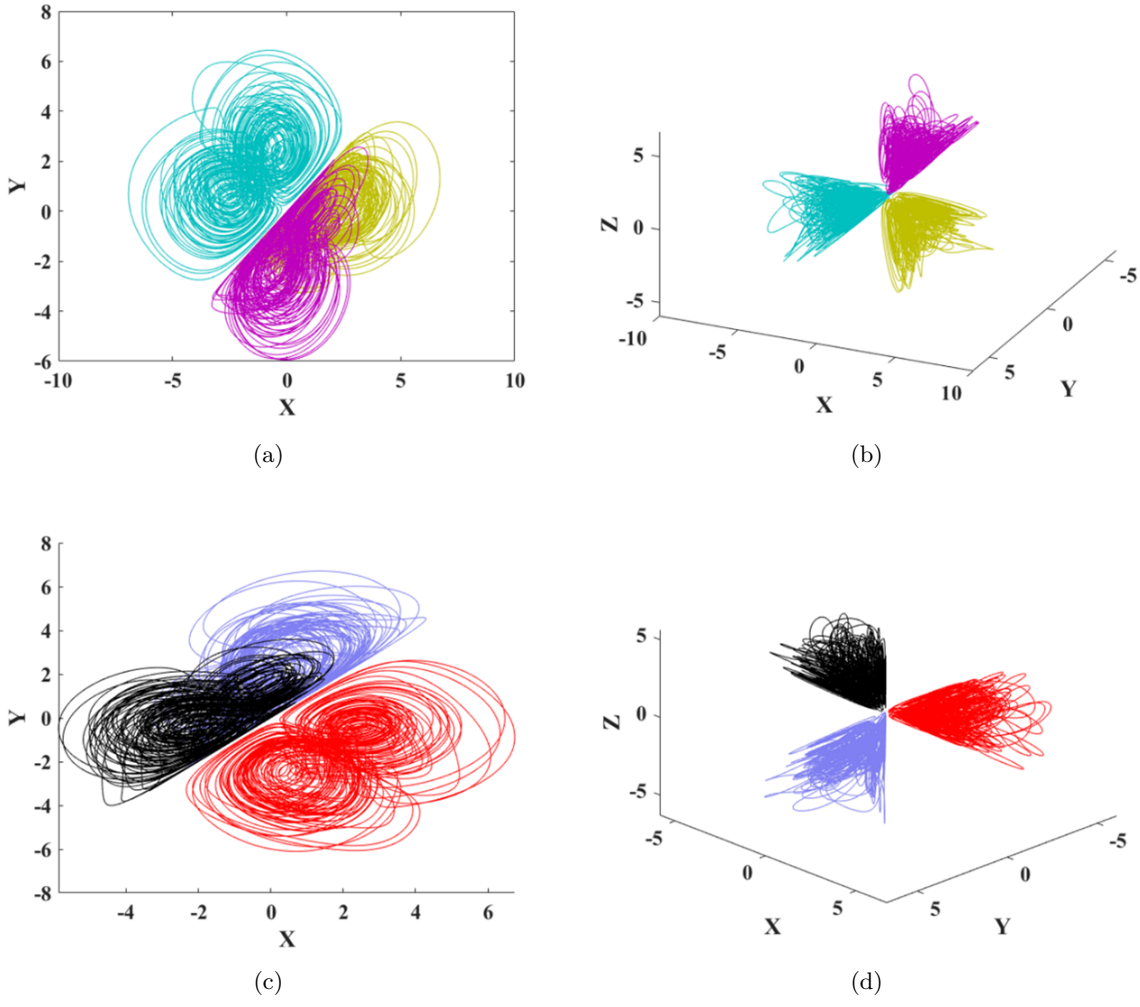

Fig. 2. Chaotic dynamics of Eq. (1) correspond to the initial conditions IC_1, IC_2, IC_3 in the first row and IC_4, IC_5, IC_6 in the second row in (a) x–y plane; (b) x–y–z space; (c) x–y plane and (d) x–y–z space.

dynamics, offering a comprehensive view of the multistable organization within the system.

3.3. *Bifurcation analysis*

To explore the dynamical transitions of the model as parameters are varied, we perform a comprehensive bifurcation analysis using forward and backward continuation techniques. In the forward (backward) continuation method, a first set of initial conditions is selected, then by increasing (decreasing), the bifurcation parameter, the initial conditions are chosen from the end of the trajectory of the previous parameter. This analysis reveals how the system's behavior changes across different parameter regimes, highlighting the emergence of various dynamics and their sensitivity to parameter perturbations. The bifurcations are plotted using three distinct initial conditions corresponding to the first group of circulant symmetric coexisting chaotic seas. The second group shows the same bifurcations as the first one.

The first case examines the effect of varying the parameter a, which is plotted with the backward reinitiation method. The bifurcation diagram presented in Fig. 3 illustrates the evolution of dynamics as a is decreased from 5 to 0. The diagram of part (a) of the figure is constructed by plotting the maximum value of the x-coordinate ($x_{\max}$) over time for each fixed value of a, using three distinct initial conditions corresponding to the first group of circulant symmetric coexisting chaotic seas. The second group shows the same bifurcations as the first one.

The bifurcation diagram in Fig. 3 illustrates that as a is decreased, the boundaries of the dynamics become smaller. This reduction in boundary size suggests a contraction of the chaotic regions,

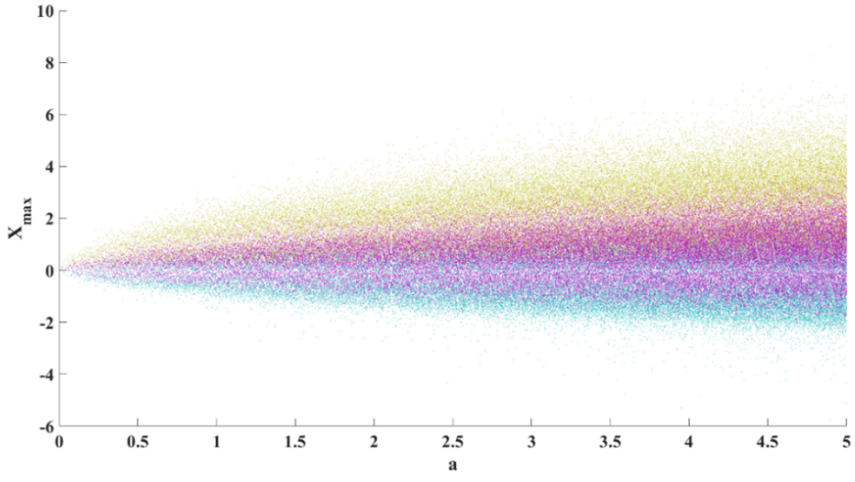

(a)

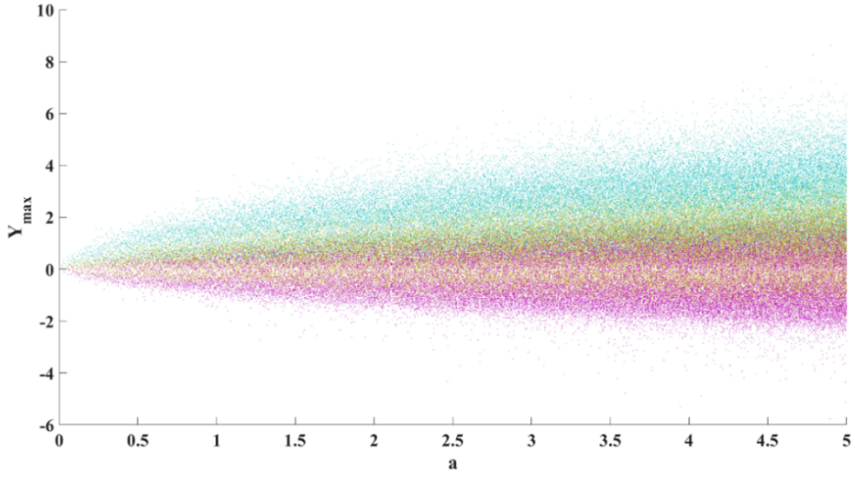

(b)

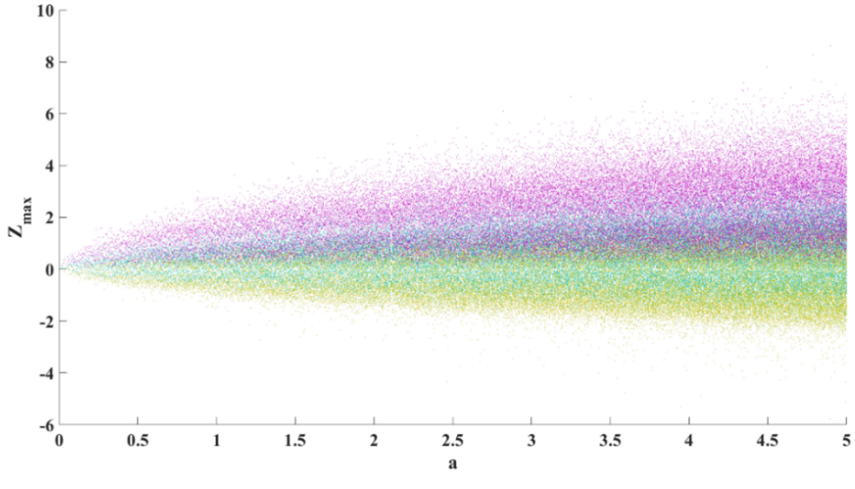

(c)

Fig. 3. Bifurcation diagram of the system by varying a with backward continuation and the first set of initial conditions $IC_1 = (-4, 5.5, 2.4)$ for azure diagram, $IC_2 = (5.5, 2.4, -4)$ for green diagram, and $IC_3 = (2.4, -4, 5.5)$ for purple diagram; (a) The maximum values of x, named $x_{\max}$; (b) $y_{\max}$ and (c) $z_{\max}$ are plotted as a function of a, showing transitions between periodic and chaotic behavior. A narrow periodic window is observed across the parameter range.

indicating a transition toward more localized or less extensive dynamics. To further elucidate the symmetry properties of the system, we compare the bifurcation diagrams for $x_{\max}$, $y_{\max}$, and $z_{\max}$. These comparisons reveal the circulant symmetry of the three dynamics of the first group. This circulant structure ensures that the dynamics of each trajectory are topologically equivalent, with their behaviors mirroring one another through cyclic variable permutations. Moreover, the consistent spacing and overlapping regions across these diagrams emphasize the multistable nature of the system, where multiple dynamics coexist under different initial conditions.

The second case involves the bifurcation diagram obtained by varying the parameter b (Fig. 4). The diagram is generated using forward continuation method, starting from $b = -1$ and employing the first initial conditions IC_1, IC_2, and IC_3, which correspond to three distinct seas belonging to the first group. As b increases, the chaotic dynamics expand, occupying increasingly larger domains in the state space.

Notably, within the interval $b \in [-0.57, -0.55]$, a significant periodic window is observed, where the system reverts to regular dynamics. This window suggests the presence of an underlying organizing structure within the chaos. The alternation between chaotic and periodic behavior across the parameter range highlights the complex interplay between stability and instability in the system.

The third case involves the bifurcation diagram derived by altering c (Fig. 5), which governs the strength of the quadratic nonlinear coupling in the system. The diagram is generated using both forward and backward continuation methods, starting from $c = 1$. Initial conditions IC_1, IC_2, and IC_3 are employed, corresponding to three distinct dynamics belonging to the first group. For values of $c < 0.99$, the system exhibits periodic behavior. These dynamics suggest stable limit cycles or regular oscillations, with trajectories converging to predictable patterns in phase space. At $c = 0.99$, a crisis occurs, marking the sudden emergence of chaotic dynamics. Notably, two other periodic windows are observed within the chaotic regime. A periodic window appears in the interval $c \in [1.76, 1.8]$, where the system temporarily reverts to regular dynamics before returning to chaos. Another periodic window is observed near the upper end of the studied interval, specifically in $c \in [2.96, 3]$. These alternating regions of chaos and periodicity highlight the complex interplay between order and disorder within the parameter space and underscore the richness of the dynamic behavior. Furthermore, the symmetry among the three dynamics is clearly reflected in the bifurcation diagrams of $x_{\max}$, $y_{\max}$, and $z_{\max}$.

The bifurcation analysis reveals a rich landscape of dynamical behavior in the proposed system, ranging from periodic motion to fully developed chaos punctuated by crisis events, abrupt transitions, and periodic windows. Each parameter variation — whether in a, b, or c — demonstrates the system's sensitivity to changes in its structure and confirms the coexistence of multiple dynamics. Notably, the circulant symmetry of the system is consistently reflected in the bifurcation diagrams, with dynamics appearing as cyclic permutations of one another. This symmetry not only enhances the visual organization of the dynamics but also underpins the system's multistability, enabling the structured coexistence of dynamics. These findings provide a deeper understanding of how symmetric nonlinear systems can support complex, yet organized, chaotic behavior — an insight with potential applications in secure communication, random number generation, and neuromorphic computing.

3.4. *Lyapunov exponent spectra*

To gain deeper insights into the dynamics of the circulant conservative chaotic system, we analyze its LEs. The LEs provide a measure of the model's sensitivity to initial conditions and help distinguish between different types of dynamics, such as periodic, chaotic, conservative, and dissipative behaviors. The results of this analysis are illustrated in Fig. 6, where we examine the variation of LEs with respect to key system parameters. The LEs are computed using the Wolf method [Wolf *et al.*, 1985] and run time 20 000.

In Fig. 6(a), the LEs of the system are presented as a function of parameter a. Throughout the studied interval, chaotic behavior is exhibited by the system, as evidenced by the presence of one positive LE. Notably, the dynamics are confirmed to be conservative, as the magnitudes of the positive and negative LEs are observed to be equal, ensuring the preservation of phase space volume.

In Fig. 6(b), the system's dynamics are studied by changing parameter b. The transition between periodic and chaotic regimes is depicted. In the

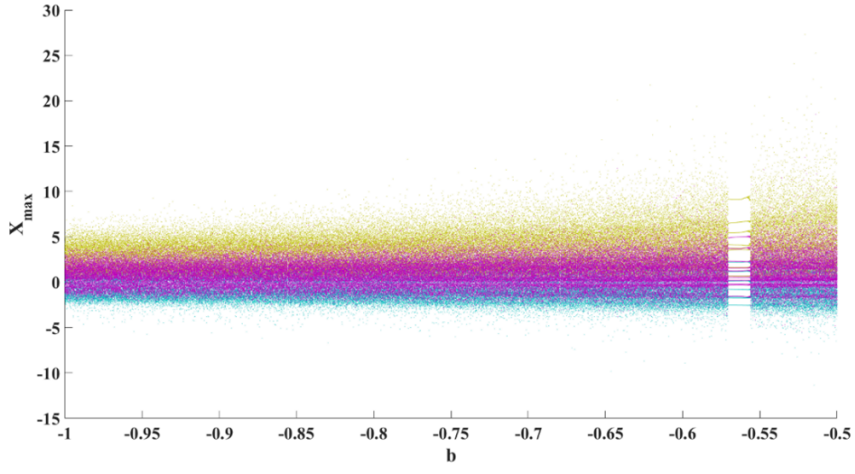

(a)

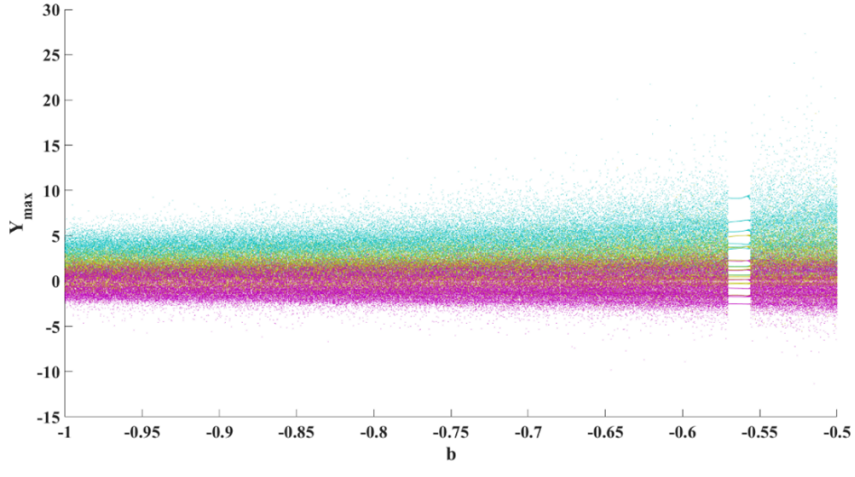

(b)

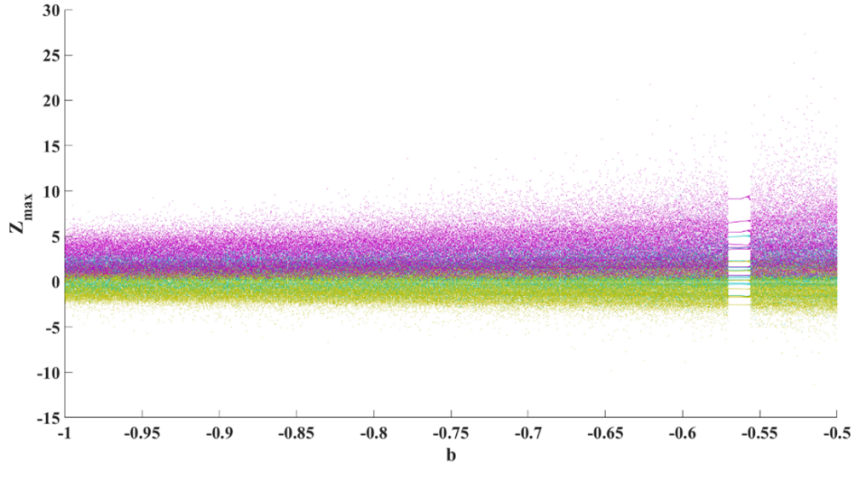

(c)

Fig. 4. Bifurcation diagrams by varying parameter b and forward continuation method and the first set of initial conditions $IC_1 = (-4, 5.5, 2.4)$ for azure diagram, $IC_2 = (5.5, 2.4, -4)$ for green diagram, and $IC_3 = (2.4, -4, 5.5)$ for purple diagram; Panels correspond to the maxima of (a) x variable; (b) y variable and (c) z variable; Periodic window and crisis are visible, indicating complex dynamical transitions.

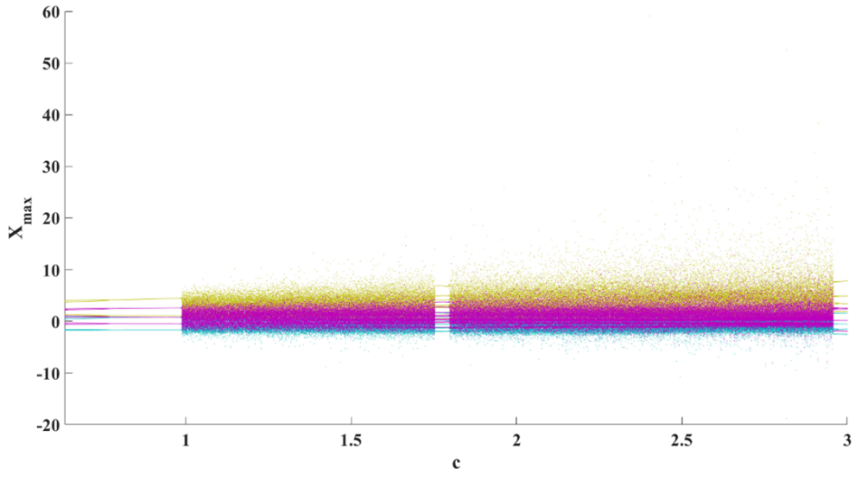

(a)

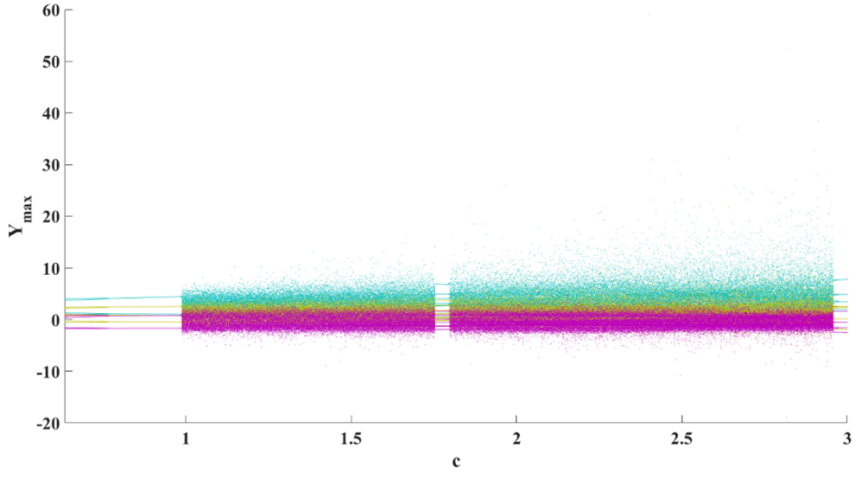

(b)

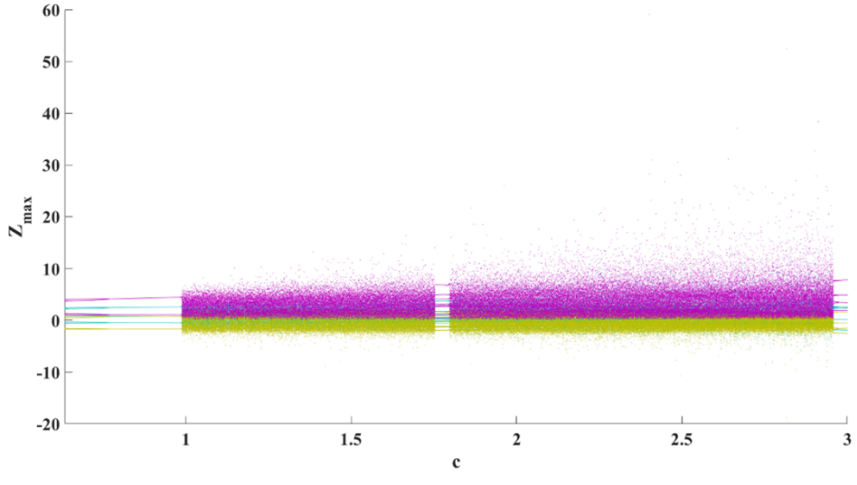

(c)

Fig. 5. Bifurcation diagrams by varying parameter c; Both forward and backward continuation methods are applied starting from $c = 1$. The first set of initial conditions are $IC_1 = (-4, 5.5, 2.4)$ for azure diagram, $IC_2 = (5.5, 2.4, -4)$ for green diagram, and $IC_3 = (2.4, -4, 5.5)$ for purple diagram. Panels correspond to the maxima of (a) x variable; (b) y variable and (c) z variable; Multiple dynamics and sharp transitions between chaotic and periodic regimes are evident.

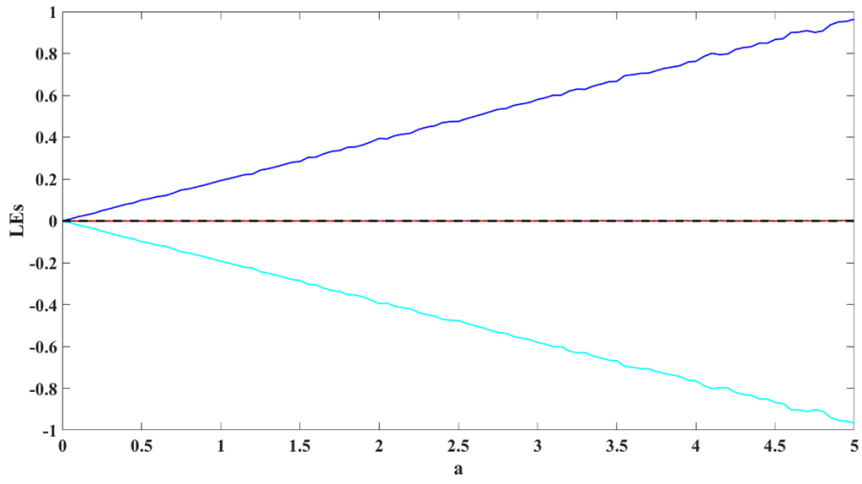

(a)

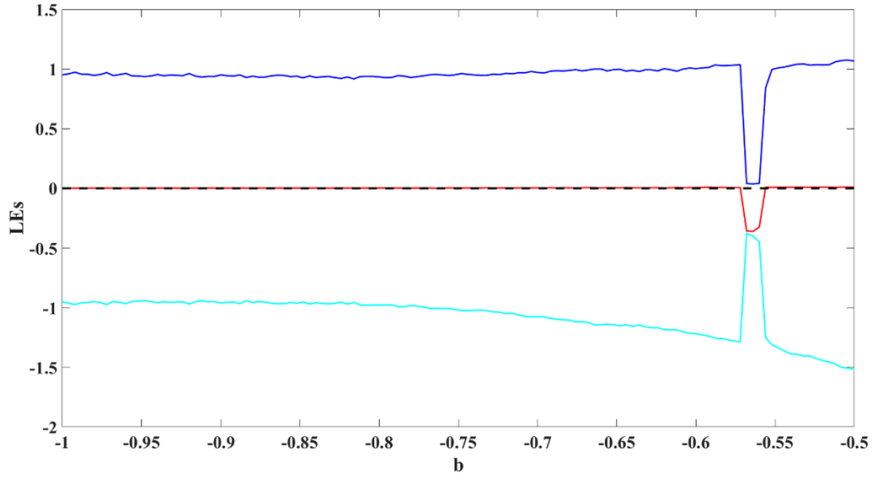

(b)

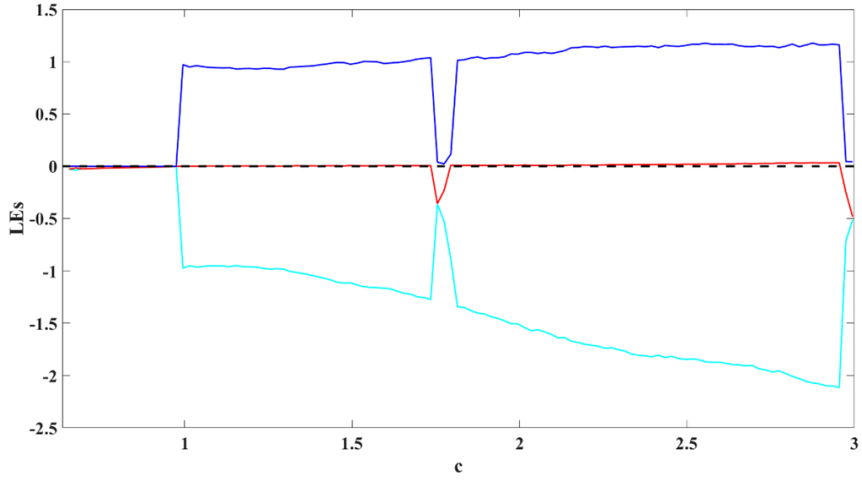

(c)

Fig. 6. LE spectra of the system; the LEs are computed as functions of parameters (a) a (b) b and (c) c, confirming the presence of chaos (positive largest LE), periodicity (zero largest LE), and conservative/dissipative transitions.

periodic regions, all LEs are found to be non-positive, indicating stable orbits. Chaotic behavior emerges when one LE becomes positive. For parameter values larger than those corresponding to the periodic window, a shift from conservative to dissipative dynamics is observed. This transition is evidenced by the imbalance between the positive and negative LEs, signifying a loss of phase space volume.

Figure 6(c) displays the LEs as a function of parameter c. Within the studied interval, a rich interplay of periodic and chaotic windows is exhibited by the system. Furthermore, the LEs reveal that in many parameter intervals, the dynamics are identified as dissipative rather than conservative. It is indicated by the presence of negative LEs that do not balance the positive ones, confirming the non-conservative nature of the system in these regions.

In summary, the diverse dynamical behaviors of the proposed system, including chaotic, periodic, conservative, and dissipative regimes, are highlighted through the LE analysis. These findings underscore the system's complexity and its potential for applications in various fields requiring rich dynamical characteristics.

4. The Region Occupied by the Chaotic Sea: A Mathematical Overview

To study the multistable nature of the proposed system, we investigate its extent of dynamics by visualizing the regions of initial conditions that result in each coexisting sea. The extent of the chaotic seas is plotted in three orthogonal planes: x_0–y_0, y_0–z_0, and z_0–x_0, as presented in Fig. 7. Each chaotic sea identified in Fig. 1 is represented using a consistent color-coding scheme, corresponding to the same sea used throughout the paper (as indicated in the color bar of Fig. 7).

One of the most striking features observed in the regions occupied by the dynamics is the presence of sharp, well-defined boundaries between the regions of different dynamics. Such crisp separations are relatively rare in complex dynamical systems, where fractal or riddled boundaries are more commonly encountered. This unusual feature suggests a high degree of structural organization within the phase space, likely stemming from the system's circulant symmetry. An additional and intriguing phenomenon revealed in the plots is the presence of dynamics associated with Color 1, which do not correspond to any of the previously identified chaotic seas. The analysis of these trajectories (for instance, in $(x_0, y_0, z_0) = (2.544, 3.936, 0)$) reveals that their LEs are all zero, indicating the absence of exponential divergence or convergence of nearby orbits. This result supports the conclusion that these trajectories lie on invariant torus rather than fixed points, limit cycles, or chaotic dynamics. The existence of such quasi-periodic structures embedded within the regions occupied by the chaotic seas highlights the richness of the system's dynamical landscape. These findings not only expand our understanding of the system's long-term dynamics but also suggest the possibility of coexisting quasi-periodic and chaotic motions, governed by the intricate interplay between symmetry, dissipation, and nonlinearity.

Let us back to the sharp boundaries between the regions occupied by the chaotic seas. We focus on the extent of the chaotic seas in the x_0–y_0 plane. Figure 8 shows the regions in five different z_0 slices. The plots are in the interval $x_0, y_0 \in [-20, 20]$. The resolution is lower than Fig. 7, so the quasi-periodic dynamics cannot be seen in it. In all of them we can see that there are some sharp lines. To discuss this line mathematically, let us get back to the saddle equilibrium points and their unstable manifolds. To understand the geometric structure underlying the sharp boundaries observed between the chaotic seas, we investigated the unstable manifolds of the system's equilibrium points. The nature of these manifolds depends on the eigenvalue spectrum at each equilibrium. For saddle points possessing a single positive real eigenvalue alongside two eigenvalues with negative real parts (either real or complex), the unstable manifold is 1D, forming a curve that emanates from the equilibrium point in the direction of the unstable eigenvector. Conversely, for saddle-focus equilibria characterized by one negative real eigenvalue and a pair of complex conjugate eigenvalues with positive real parts, the unstable manifold is 2D, forming a surface (or plane locally) spanned by the real and imaginary parts of the eigenvector associated with the unstable complex eigenvalue. The computed manifolds provide crucial insight into the organization of phase space and the origin of the boundaries between distinct dynamical regions.

To understand the geometric structure underlying the sharp boundaries observed between the chaotic seas, we investigate the unstable manifolds

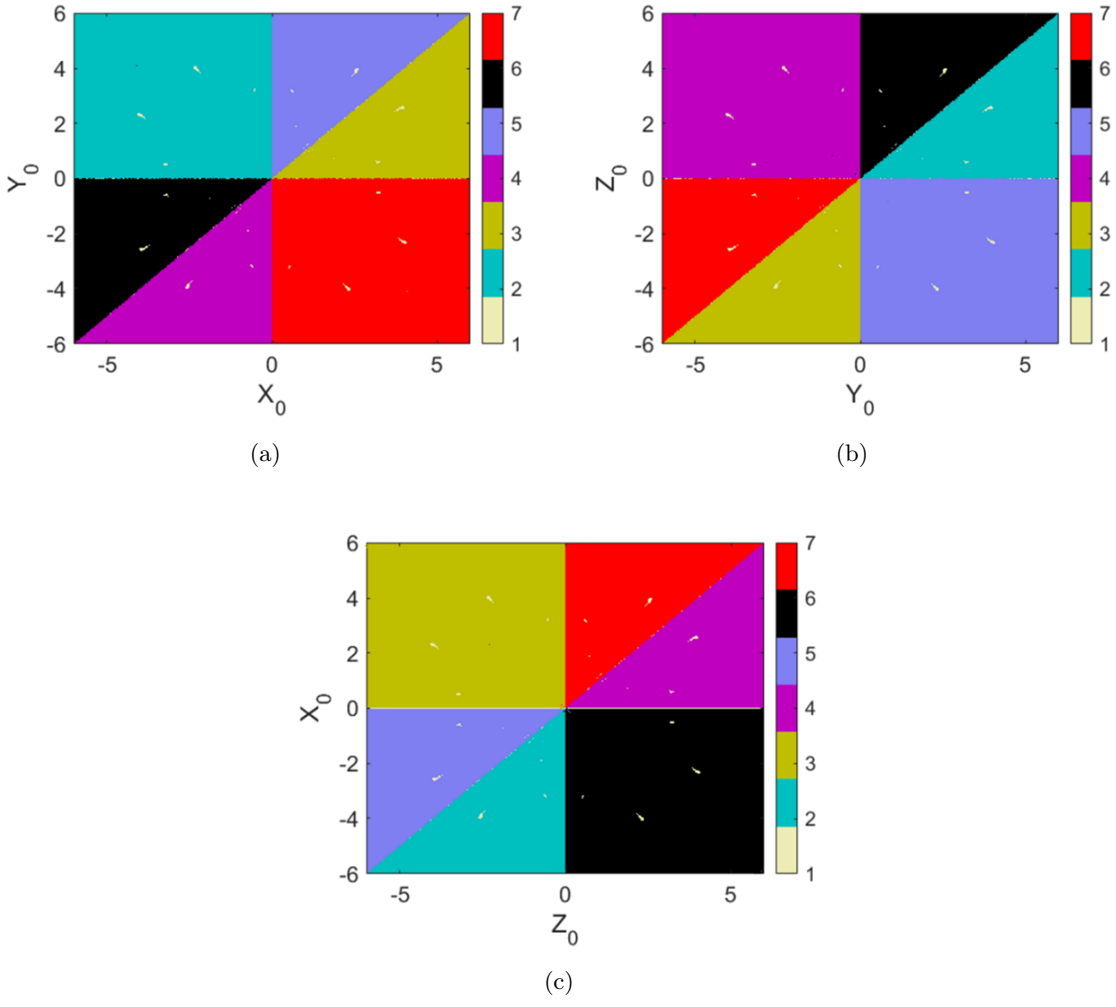

Fig. 7. The extent of the dynamics projected onto (a) x_0–y_0, (b) y_0–z_0 and (c) z_0–x_0 planes; each color represents the region occupied by a chaotic sea with the same color, except for color 1, which corresponds to quasi-periodic invariant tori embedded within the chaotic regions. Sharp boundaries between the regions occupied by the chaotic seas are observed, a rare feature in nonlinear systems.

of the model's equilibria. The nature of these manifolds depends on the eigenvalue spectrum at each equilibrium. For saddle points possessing a single positive real eigenvalue alongside two eigenvalues with negative real parts (either real or complex), the unstable manifold is 1D, forming a curve that emanates from the equilibrium point in the direction of the unstable eigenvector. The equation of such a 1D unstable manifold (line) passing through an equilibrium point $\mathbf{p} = (p^1, p^2, p^3)$ in the direction of eigenvector $\mathbf{v} = (v^1, v^2, v^3)$ is given by $\frac{x-p_1}{v_1} = \frac{y-p_2}{v_2} = \frac{z-p_3}{v_3}$. Conversely, for saddle-focus equilibria characterized by one negative real eigenvalue and a pair of complex conjugate eigenvalues with positive real parts, the unstable manifold is 2D, forming a surface (or plane locally) spanned by the real and imaginary parts of the eigenvector associated with the unstable complex eigenvalue. If $\mathbf{v} = \mathbf{v}_r + i\mathbf{v}_i$ is the complex eigenvector corresponding to eigenvalue $\lambda = \alpha + i\beta$ (where $\alpha > 0$), then the 2D unstable manifold is spanned by the real vectors $\mathbf{v}_r$ and $\mathbf{v}_i$. The equation of this unstable plane passing through equilibrium point p is $a(x-p_1) + b(y-p_2) + c(z-p_3) = 0$, where (a, b, c) is the normal vector to the plane, obtained from $\mathbf{n} = \mathbf{v}_r \times \mathbf{v}_i$.

These unstable manifolds are computed by numerically determining the eigenvectors corresponding to the unstable eigenvalues of key equilibrium points. For 2D manifolds, we constructed the spanning plane using the real and imaginary parts of the complex eigenvectors. The computed

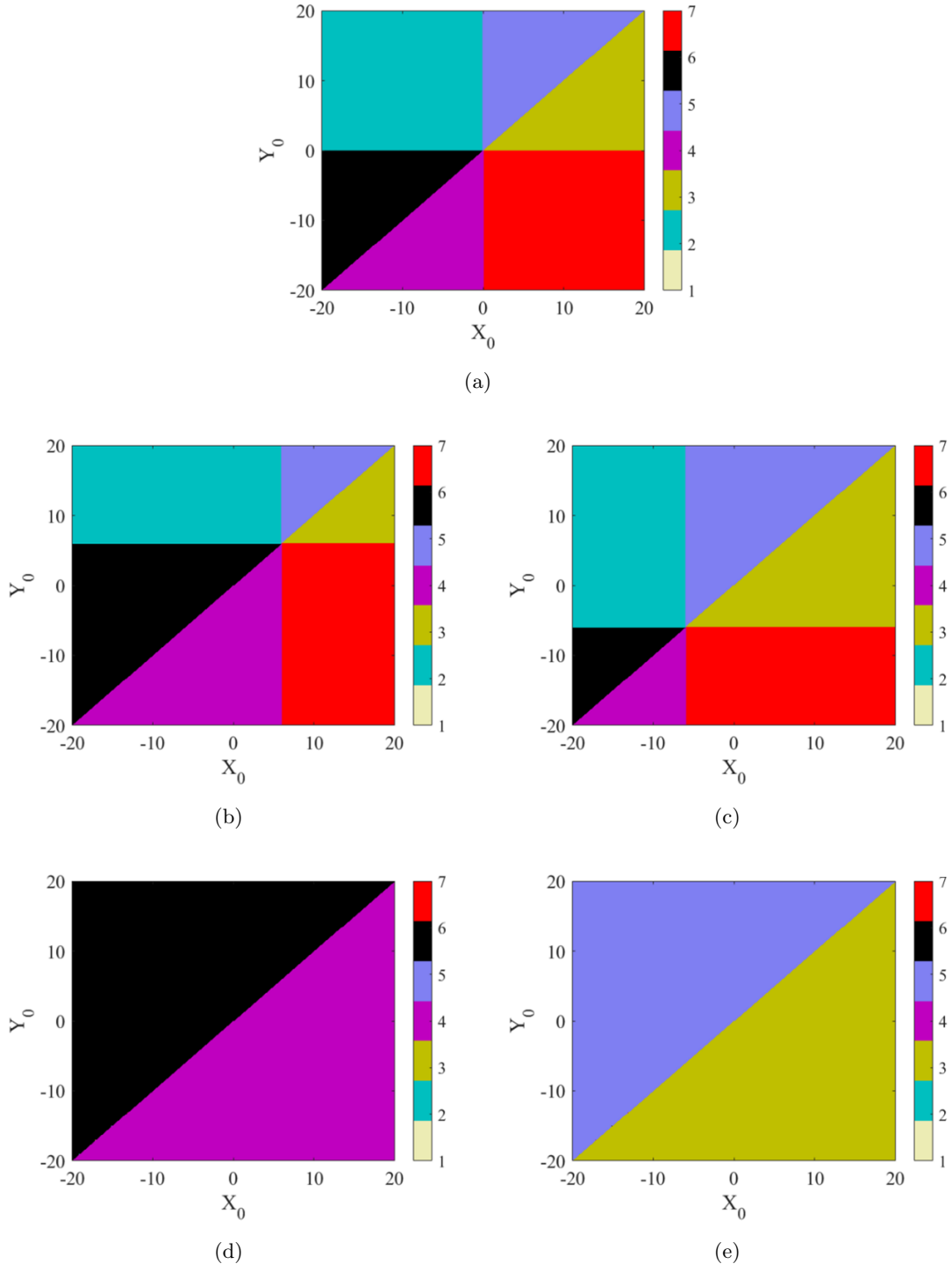

Fig. 8. The extent of the dynamics projected onto the x_0–y_0 planes in the intervals $[-20, 20]$ and (a) $z_0 = 0$; (b) $z_0 = 6$; (c) $z_0 = -6$; (d) $z_0 = 30$ and (e) $z_0 = -30$; each color represents the region occupied by a chaotic sea with the same color; compared to Fig. 7, smaller resolution is used in this figure, so the small quasi-periodic points cannot be seen in it.

manifolds provide crucial insight into the organization of phase space and the origin of the boundaries between distinct dynamical regions, with the 1D and 2D unstable manifolds forming the sharp linear boundaries observed in Fig. 8.

Let us focus on specific equilibrium points and their corresponding unstable manifolds in relation to the observed boundaries. Consider Eq_1, located at the origin $(0, 0, 0)$ within the $z_0 = 0$ plane, which possesses one positive eigenvalue. Consequently, its

unstable manifold is 1D, forming a line with the equation $x = y = z$. This line intersects all the x_0–y_0 planes shown in Fig. 8, marking the center of the color divisions. While this relationship is evident far from Eq_1, its direct influence is expected to be most pronounced in its immediate vicinity.

Next, we examine Eq_9 and Eq_{10}, also located in the $z_0 = 0$ plane. These equilibrium points possess two complex conjugate eigenvalues with positive real parts, resulting in 2D unstable manifolds (planes). The equations of these unstable planes are $x = z$ and $y = z$, respectively. The intersections of these planes with the x_0–y_0 planes at various z_0 values precisely correspond to the boundaries defined by $x = z_0$ and $y = z_0$, as observed in Fig. 8.

Further analysis of Eq_8, though not located in the x_0–y_0 planes of Fig. 8, reveals its influence in Figs. 7(b) and 7(c). Its unstable manifold forms a plane with the equation $x = y$. Notably, although these manifold calculations are inherently local, the intersection of this plane with the $z_0 = 0$ plane is clearly visible in our analysis, reinforcing the connection between the theoretical manifolds and the observed boundaries. In contrast, equilibrium points Eq_2 through Eq_7 are not located in our studied x_0–y_0 planes. Their 1D unstable manifolds do not directly intersect the planes shown in Fig. 8. However, for completeness, the equations of their unstable lines are: Eq_2: $x = -1.2910$, $z = 5.1640 - y$; Eq_3: $z = -1.2910$, $x = 5.1640 - y$; Eq_4: $y = -1.2910$, $x = 5.1640 - z$; Eq_5: $x = 1.2910$, $y = -5.1640 - z$; Eq_6: $z = 1.2910$, $y = -5.1640 - x$; Eq_7: $y = 1.2910$, $z = -5.1640 - x$.

5. Conclusion

In this work, we introduced and analyzed a novel 3D-chaotic system characterized by circulant symmetry, and six coexisting chaotic seas. The system's governing equations incorporated cubic nonlinearities, which give rise to complex stretching and folding mechanisms essential for chaos generation. Through comprehensive numerical analysis, several unique dynamical features were revealed. The system supported six distinct chaotic dynamics categorized into two groups, each associated with a different set of initial conditions. The dynamics of the two groups were symmetrically arranged around the origin. In each group, the three seas were related to one another through cyclic permutations of the state variables. The regions occupied by the seas exhibited sharp, well-defined boundaries — a rare phenomenon in nonlinear dynamical systems — indicating a high degree of structural organization within the phase space. The sharp boundaries of the regions were mathematically discussed by the help of unstable manifolds of saddle equilibrium points. Embedded within the regions occupied by the chaotic sea, we identified invariant tori, where trajectories display quasi-periodic motion. These structures suggested the coexistence of quasi-periodic and chaotic dynamics, further enriching the complexity of the system's behavior. Bifurcation diagrams obtained by varying parameters a, b, and c revealed rich transitions between periodic, chaotic, conservative, and dissipative regimes, punctuated by crisis events and periodic windows. The LE spectra confirmed the chaotic nature of the dynamics and demonstrated the system's ability to transition smoothly between conservative and dissipative dynamics, depending on parameter values.

The multistable and symmetry-organized nature of the proposed system not only enriches the theoretical understanding of structured chaos but also opens promising avenues for practical implementation. In particular, the coexistence of six well-separated chaotic seas — coupled with sharp basin boundaries and circulant symmetry — makes the system highly suitable for control and synchronization strategies, which are essential for applications such as secure communication, chaos-based encryption, and neuromorphic computing. Future work will focus on developing adaptive control laws and synchronization protocols to enable reliable switching among coexisting seas, as well as hardware realization via analog or digital circuits.

In summary, this work advances the understanding of symmetric chaotic systems and introduces a new paradigm for studying multistability, conservation laws, and structured chaos. By combining mathematical rigor with aesthetic appeal, it opens exciting avenues for both theoretical exploration and technological innovation.

Author's Contributions

Karthikeyan Rajagopal: Conceptualization, investigation, writing – original draft.
Fahimeh Nazarimehr: Conceptualization, methodology, writing – original draft.
Sajad Jafari: Methodology, validation, writing – review & editing.
Julien C. Sprott: Software, supervision, writing – review & editing.

Conflict of Interest

The authors declare that they have no conflict of interest.

Data Availability

Data generated during this study will be made available on reasonable request.

ORCID

Karthikeyan Rajagopal
https://orcid.org/0000-0003-2993-7182
Fahimeh Nazarimehr
https://orcid.org/0000-0002-2664-9006
Sajad Jafari
https://orcid.org/0000-0002-6845-7539
Julien C. Sprott
https://orcid.org/0000-0001-7014-3283

References

Azam, A., Sunny, D. A. & Aqeel, M. [2022] "Generation of multiscroll chaotic attractors of a finance system with mirror symmetry," *Soft Comput.* **27**, 2769–2782.

Bao, B., Zhou, C., Bao, H., Chen, B. & Chen, M. [2025] "Heterogeneous Hopfield neural network with analog implementation," *Chaos Solit. Fract.* **194**, 116234.

Barathi, G., Natiq, H., He, S., Wang, H., Rajagopal, K. & Hussain, I. [2025] "A novel dynamical system: Chaos, hidden dynamics, multistability, and applications," *Int. J. Bifurcation and Chaos* **35**, 2530015.

Chen, L., Bao, H., Zhang, X., Zhang, Y. & Bao, B. [2025] "DC-bias induced chaotic dynamics and periodic bursting in Chua's diode-based FitzHugh–Nagumo circuit," *Chaos Solit. Fract.* **199**, 116739.

Kopparthi, V. R., Kali, A., Sabat, S. L., Anumandla, K. K., Peesapati, R. & Fouda, J. A. E. [2022] "Hardware architecture of a digital piecewise linear chaotic map with perturbation for pseudorandom number generation," *AEU-Int. J. Electron. Commun.* **147**, 154138.

Li, H., Hua, Z., Bao, H., Zhu, L., Chen, M. & Bao, B. [2020a] "Two-dimensional memristive hyperchaotic maps and application in secure communication," *IEEE Trans. Ind. Electron.* **68**, 9931–9940.

Li, C., Sun, J., Sprott, J. C. & Lei, T. [2020b] "Hidden attractors with conditional symmetry," *Int. J. Bifurcation and Chaos* **30**, 2030042.

Obaid, M. J., Neamah, A. A., Shukur, A., Pham, V.-T. & Grassi, G. [2025] "A reliable color image encryption scheme based on a novel dual-wing hyperchaotic map," *Expert Syst. Appl.* **289**, 128237.

Sprott, J. C. [2010] *Elegant Chaos*: *Algebraically Simple Chaotic Flows* (World Scientific).

Sprott, J. C. [2011] "A proposed standard for the publication of new chaotic systems," *Int. J. Bifurcation and Chaos* **21**, 2391–2394.

Tamba, V. K., Pham, V.-T. & Volos, C. [2025] "A simple third-order Hopfield neural network: Dynamic analysis, microcontroller implementation and application to random number generation," *Symmetry* **17**, 330.

Vaidyanathan, S., He, S. & Simbas, A. [2021] "A new multistable double-scroll 4-D hyperchaotic system with no equilibrium point, its bifurcation analysis, synchronization and circuit design," *Arch. Control Sci.* **31**, 99–128.

Vignesh, D., He, S. & Banerjee, S. [2025] "A review on the complexities of brain activity: Insights from nonlinear dynamics in neuroscience," *Nonlin. Dyn.* **113**, 4531–4552.

Wang, R., Li, C., Kong, S., Jiang, Y. & Lei, T. [2022] "A 3D memristive chaotic system with conditional symmetry," *Chaos Solit. Fract.* **158**, 111992.

Wang, N., Cui, M., Yu, X., Shan, Y. & Xu, Q. [2024] "Generation of no-equilibrium multi-fold chaotic attractor for image processing and security," *Appl. Math. Model.* **133**, 271–285.

Wolf, A., Swift, J. B., Swinney, H. L. & Vastano, J. A. [1985] "Determining Lyapunov exponents from a time series," *Physica D* **16**, 285–317.

Xu, Q., Tan, X., Zhu, D., Bao, H., Hu, Y. & Bao, B. [2020] "Bifurcations to bursting and spiking in the Chay neuron and their validation in a digital circuit," *Chaos Solit. Fract.* **141**, 110353.

Xu, Q., Huang, L., Wang, N., Bao, H., Wu, H. & Chen, M. [2023a] "Initial-offset-boosted coexisting hyperchaos in a 2D memristive Chialvo neuron map and its application in image encryption," *Nonlin. Dyn.* **111**, 20447–20463.

Xu, Q., Wang, Y., Chen, B., Li, Z. & Wang, N. [2023b] "Firing pattern in a memristive Hodgkin–Huxley circuit: Numerical simulation and analog circuit validation," *Chaos Solit. Fract.* **172**, 113627.

Xu, Q., Wang, Y., Iu, H. H. C., Wang, N. & Bao, H. [2023c] "Locally active memristor-based neuromorphic circuit: Firing pattern and hardware experiment," *IEEE Trans. Circuits Syst.-I*: *Regul. Pap.* **70**, 3130–3141.

Yang, Y., Huang, L., Xiang, J., Bao, H. & Li, H. [2021] "Design of multi-wing 3D chaotic systems with only stable equilibria or no equilibrium point using rotation symmetry," *AEU-Int. J. Electron. Commun.* **135**, 153710.

Yousfi, H., Islam, Y., He, S., Gasri, A. & Hassan, M. M. [2024] "Advanced medical image encryption techniques using the fractional-order Halvorsen circulant systems: Dynamics, control, synchronization and security applications," *Phys. Scr.* **99**, 055208.